Effect of annealing temperature on the structural and magnetic properties of Ni-Co-Fe-Al-O ferrite

Nehal Ahmed[a], G. H. Kale[b], V. B. Kawade[c], Y. A. Vijapure[d], R. H. Kadam[e], Jaishree Bhale[f] S. B. Shelke[a*]

[a]Physics Department, S. M. P. College, Murum, Dist. Osmanabad (M.S.) India

[b]Electronics Department, Y. C. College, Tuljapur, Dist. Osmanabad (M.S.) India

[c]Physics Department, L. L. D. M. Mahavidyalaya, Parali (V), Dist. Beed (M.S.) India

[d]Chemistry Department, Shrikrishna Mahavidyalaya, Gunjoti, Dist. Osmanabad (M.S.) India

[e]Physics Department, Shrikrishna Mahavidyalaya, Gunjoti, Dist. Osmanabad (M.S.) India

[f]Govt. Holkar science College,Indore(M.P.)India

Abstract

Nanocrystalline powder of the composition $Ni_{0.5}Co_{0.5}FeAlO_4$ was successfully obtained by using sol-gel auto-combustion technique. The decomposition pattern was obtained by using thermo-gravimetric analysis. The X-ray diffraction patterns shows the reflections for the planes (220), (311), (222), (422), (333), (440) and (533) which confirms the cubic spine structure of the present samples. By using the XRD data the structural parameters like lattice parameter, X-ray density, percentage porosity and crystallite size was obtained. The average grain size obtained from SEM micrographs shows minimum size (76nm) at lower temperature (500^0C).and minimum size for higher temperature (800^0C) (139nm). The hysteresis curves show normal ferrimagnetic behaviour for all the samples. For lower sintering temperature the saturation magnetization is least while as it increases with increase in sintering temperature and shows highest value for the sintering temperature 800^0C. The magnetic moment increases with increasing sintering temperature.

Keywords: *Annealing temperature, lattice constant, and saturation magnetization.*

Introduction:

Nickel ferrite and cobalt ferrites are the well known examples of inverse spinel structures. In particular pure and substituted nickel ferrites are technologically important materials and have been studied by several researchers [1-4]. Cobalt ferrite is technologically important in various applications due to its very high coercivity, low losses of eddy currents and high saturation magnetization. Several researcher have been reported the results of pure and substituted nickel and cobalt ferrites [1, 5-8]. Nickel ferrites with aluminium substitution shows a broad range of applications in radio and microwave frequencies, where the electrical and magnetic losses are required to be minimum [1, 19-10]. The addition of aluminium results in increasing

the resistivity which decreases the dielectric losses and saturation magnetization. Sintering temperature and synthesis rout plays important role in the fabrication of nano-structured ferrite materials. Attempts are made to synthesis the ferrites by changing their sintering temperature and synthesis route in order to study the structural, electrical and magnetic properties [11-14].

In the present investigation we have prepared the nanocrystalline powder of Ni-Co-Fe-Al-O ferrite and sintered at four different temperature 500^0C, 600^0C, 700^0C and 800^0C. Effect of sintering temperature on the structural and magnetic properties of Ni-Co-Fe-Al-O ferrite nanoparticles was studied.

Sample preparation:

Nickel nitrate ($Ni(NO_3)_2 \cdot 3H_2O$), cobalt nitrate ($Co(NO_3)_2 \cdot 3H_2O$), ferric nitrate ($Fe(NO_3)_3 \cdot 9H_2O$), aluminum nitrate ($Al(NO_3)_3 \cdot 9H_2O$), citric acid ($C_6H_8O_7 \cdot H_2O$) with high purity (99% pure) were used as initial materials for the synthesis of $Ni_{0.5}Co_{0.5}FeAlO_4$ ferrite nanoparticles via sol-gel route. Whole reaction was carried out in air atmosphere without protection of inert gases. All metal nitrates were mixed thoroughly in double distilled water and citric acid was mixed in the solution by taking the molar ratio of citric acid with metal nitrates as 1:3 with their weight proportion. The whole mixture is kept on magnetic stirrer with hot plate. To maintain the pH = 7 of the solution, liquid ammonia was poured slowly with continuous stirring the mixture until the pH maintains at 7. Along with continuous stirring, the mixture is then heated at constant temperature of 90^0C. Due to heat treatment evaporations process starts and after some time the mixed solution was converted into viscous sol and finally converted in to viscous brown gel. After removal of water content from the mixture the dark brown gel was self ignited and burnt with glowing flints. In the decomposition process the entire citrate complex was totally consumed and the auto-combustion process was completed. Finally, the brown colored ash was obtained as a yield of the auto-combustion process which can be called as ‘precursor’. The final powder was divided into four equal parts and subjected to final sintering at four different temperatures 500^0C, 600^0C, 700^0C and 800^0C respectively.

Experimental:

The dried gels were characterized via thermo gravimetric (TGA) at a heating rate of 10^0C /min in air atmosphere. By using the TG curve the exact temperature of formation of ferrite phase was obtained. The final powders of $Co_{0.5}Ni_{0.5}FeAlO_4$ sintered at four different temperatures 500^0C to 800^0C in the step of

100^0C for 6 hrs each are characterized X-ray diffraction technique. Phillips X-ray diffractometer (Model 3710) was used to obtain the XRD plots of all the samples. The radiation used for diffraction was Cu-k_α having the wavelength λ = 1.5405Å. The scanning rate was 4.26^0/min and the scanning rate was 0.02^0. The X-ray generator was operated at 40kV and 30mA. The microstructure of and morphology of sintered powders were characterized by field effect scanning electron microscopy (FE-SEM) on JEOL-JSM-5600 N scanning electron microscope.

Magnetic measurements were performed using the commercial PARC EG&G vibrating sample magnetometer VSM 4500. Magnetic hysteresis loops were measured at room temperature with maximum applied magnetic fields up to 0.95 T. Magnetic field sweep rate was 5 Oe/S for all measurements. Hence measurement of hysteresis loops with maximum field of 0.95 T took about 3 hr. The samples prepared in powder form were fixed in paraffin in order to exclude the motion of powder in a measuring cap.

Results and discussion:

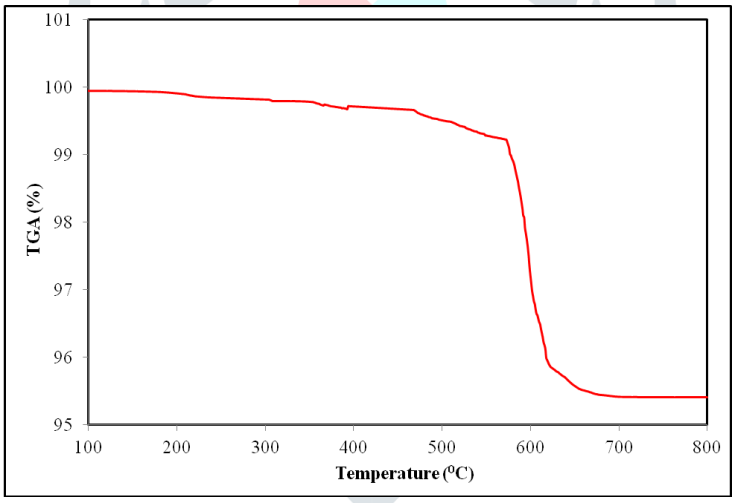

Fig. 1: TG curve of $Ni_{0.5}Co_{0.5}FeAlO_4$

Fig. 1 shows the TG curve of the sample $Ni_{0.5}Co_{0.5}FeAlO_4$ prepared via sol-gel auto-combustion technique. It is observed that between the temperatures 300^0C to 650^0C the weight loss is major. This loss is may be related to the reaction between initial materials and the water content will be completely removed between the temperature range room temperature to 300^0C. After the temperature 300^0C, the organic derivatives and citric acid will be decomposed and the weight loss is observed. Above the temperature 650^0C the weight loss is very negligible and shows almost straight line trend. At this temperature, crystallization of the sample was takes place completely and pure ferrite phase was obtained.

Fig. 2 shows the X-ray diffraction patterns for the samples of $Ni_{0.5}Co_{0.5}FeAlO_4$ sintered at 500^0C, 600^0C, 700^0C and 800^0C. XRD peaks clearly shows that, for all the samples (except plot A), reflections are occurred for the planes (220), (311), (222), (422), (333), (440) and (533). The reflection planes confirm the single phase cubic spinel structure of the samples. A careful observation of XRD patterns shows that the intensity of reflection peaks increases with the increase in sintering temperature. Also, the sharpness of most intensive peak (311) increases with increase in sintering temperature which indicates that the particle size increases with temperature.

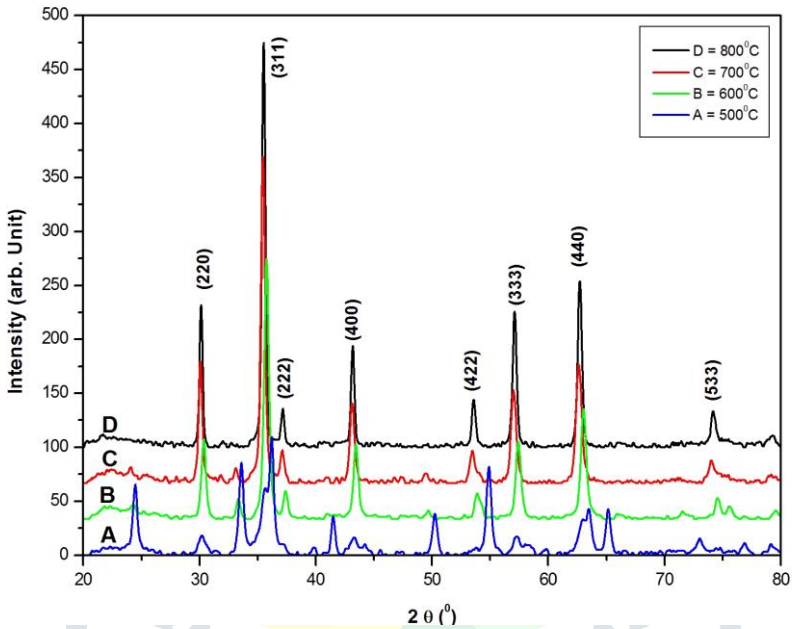

Fig. 2: X-ray diffraction plots of $Ni_{0.5}Co_{0.5}FeAlO_4$

By using the values of interplanner spacing's in the following relation for cubic structures, the lattice parameter 'a' was calculated [15].

$$a = d\sqrt{\left(h^2 + k^2 + l^2\right)} \qquad (1)$$

Where, notations have their usual meaning. For every plane, lattice constant was calculated and the average was considered for further calculations. The values of average lattices constant are given in Table 1. The value of lattice constant for the sample sintered at 500^0C is found 8.3766 Å and as sintering temperature increases, it increases and finally obtained 8.3910Å for the sample sintered at 800^0C. Similar behaviour of the lattice constant was observed in literature also [16].

Table 1: Lattice parameter 'a', X-ray density 'd_x', Particle size 'D', Bulk density 'd_B', porosity 'P' and surface area 'S' for $Ni_{0.5}Co_{0.5}FeAlO_4$.

Sintering Temperature T (°C)	a (Å)	dx (g/cm^3)	D (nm)	d_B (g/cm^3)	P (%)	S (m^2/g)
500	8.3766	4.6411	18.31	3.4621	34.05	94.66
600	8.3808	4.6341	20.95	3.5517	30.47	80.65
700	8.3899	4.6191	24.59	3.6253	27.41	67.31
800	8.3910	4.6172	29.75	3.7557	22.94	53.71

The X-ray density 'd_X' was calculated by putting the values of molecular weight and unit cell volume in the following relation;

$$d_x = \frac{8M}{NV} \qquad (2)$$

Where, M is the molecular weight of the composition, N is the Avogadro's number ($6.022140857 \times 10^{23}$ $mole^{-1}$) and V is the unit cell volume which is nothing but cube of lattice parameter for cubic structures ($V = a^3$). The calculated values of X-ray density are given in Table 4.2. X-ray density decreases with increase in sintering temperature. This decrease in bulk density is attributed to the increase in lattice parameter which increases the unit cell volume. By using the mass-volume relation, bulk density was calculated and the values obtained are given in Table 1.

The percentage porosity of all the samples was calculated by inserting the values of bulk density and X-ray density in the following relation [17],

$$P(\%) = \left(\frac{d_{X-ray} - d_{Bulk}}{d_{Bulk}} \right) \times 100 \qquad (3)$$

Table 1, represents the calculated values of percentage porosity of $Ni_{0.5}Co_{0.5}FeAlO_4$ as a function of sintering temperature. Increase in sintering temperatures decreases the porosity of the samples which is related to the increase in bulk density of the samples and crystalline size. To estimate the average crystalline size from the XRD data, following Scherer's formula was used,

$$D_{XRD} = \frac{k\lambda}{\beta Cos\theta_B} \qquad (4)$$

Where, D_{XRD} is the average crystalline size obtained from XRD data, k is the constant (0.9), λ = wavelength of the incident radiation (=1.5405Å), β is FWHM (Full width of half maxima) and θ_B is the diffraction angle. Calculated values of crystalline size for all the samples are given in Table 1. As the sintering temperature increases, the line broadening of XRD peaks decreases and the sharp peaks are observed. The decrease in line broadening of peaks decreases the crystallite size.

The specific surface area of all the samples was calculated by using the following relation [18],

$$S = \frac{6000}{D\rho_A} \qquad (5)$$

Where, S is specific surface area, D is the diameter of the crystallite and ρ_A is the density measured in gms/cm^3. Table 1 reflects the values of specific surface area 'S' with sintering temperature. Specific surface area 'S' increases with increase in sintering temperature.

Scanning electron micrographs of two samples (initial and final) are shown in Fig. 3. The sintering temperature greatly affects the structure of the samples. The keen observation of the micrographs shows that the surface of the samples demonstrates well-defined grains along with few pairs. May be due to the heat treatment at different temperatures, some voids are also observed in images [19]. The average grain size obtained from SEM micrographs shows minimum size (76nm) at lower temperature (500^{0}C).and minimum size for higher temperature (800^{0}C) (139nm). No linear variation is observed in the values of average grain size as a function of temperature.

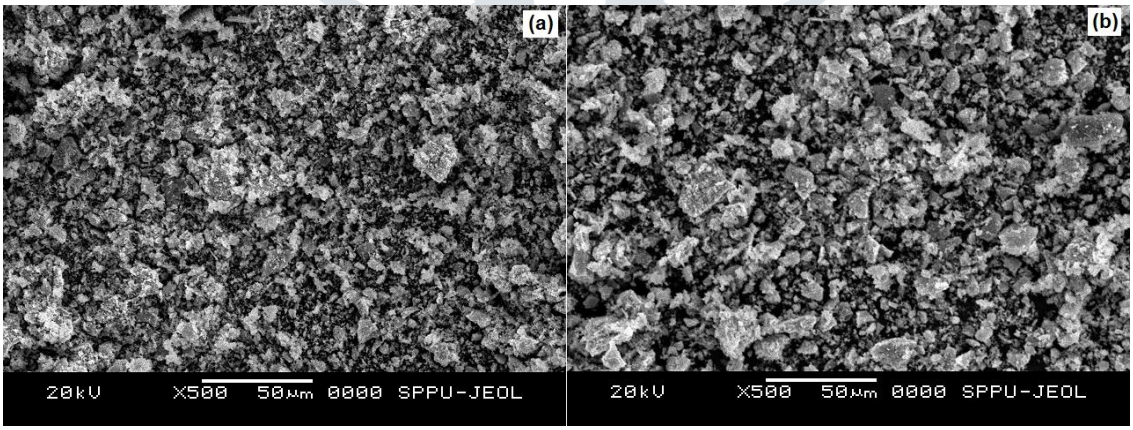

Fig. 3: Scanning electron micrographs of $Ni_{0.5}Co_{0.5}FeAlO_4$ a) 500^{0}C, b) 800^{0}C

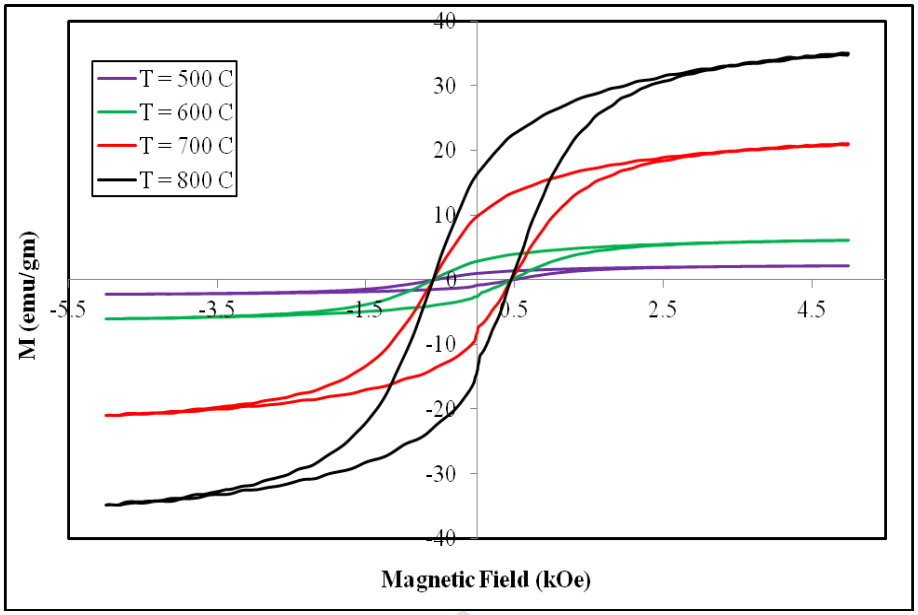

Fig. 4: Hysteresis curves of $Ni_{0.5}Co_{0.5}FeAlO_4$

Fig. 4 represents the hysteresis curves of all the samples of $Ni_{0.5}Co_{0.5}FeAlO_4$. The hysteresis curves show normal ferrimagnetic behaviour for all the samples. The magnetic parameters viz. saturation magnetization, magneton number remnant magnetization, coercivity etc. are obtained from the hysteresis curves. For lower sintering temperature the saturation magnetization is least while as it increases with increase in sintering temperature and shows highest value for the sintering temperature 800^0C. The values of saturation magnetization with sintering temperature are given in Table 2. Similar behaviour of saturation magnetization with sintering temperature is observed in literature also [19-21]. Under the action of an applied magnetic field the coercive field is nothing but the measure of magnetization reversal process. Coercive field depends mainly on the crystalline anisotropy, particle size and domain structure of the material. Because of strong crystalline anisotropy associated with Co atoms, cobalt ferrite is commonly known for the high coercivity [22]. In the present case, coercivity of $Ni_{0.5}Co_{0.5}FeAlO_4$ increases with increase in sintering temperature and the values are given in Table 2. The squareness (R) of the hysteresis curve [23], i.e. the ratio of remnant magnetization to saturation magnetization is calculated and given in Table 2. The values of R are found almost same for all the samples; this is may be due to the increasing trend of both M_S and M_R in the same proportion.

Table 2: Saturation magnetization, remnant magnetization, remnant ratio, coercivity and magnetic moment for $Ni_{0.5}Co_{0.5}FeAlO_4$

Sintering Temperature T (°C)	Saturation magnetization 'M_S' (emu/gm)	Remnant Magnetization 'M_R' (emu/gm)	Remnant ration 'R'	Coercivity 'H_C' (Oe)
500	2.2057	1.0833	0.4911	871
600	6.0786	2.9248	0.4812	921
700	21.086	10.359	0.4913	1064
800	35.003	17.1965	0.4913	1127

Conclusions:

Nanocrystalline powder of the composition $Ni_{0.5}Co_{0.5}FeAlO_4$ was successfully obtained by using sol-gel auto-combustion technique. By the thermo-gravimetric analysis, it was clear that the pure ferrite phase was obtained nearly at 600^0C. As the sintering temperature increases, the line broadening of XRD peaks decreases and the sharp peaks are observed. The hysteresis curves show normal ferrimagnetic behaviour for all the samples. For lower sintering temperature the saturation magnetization is least while as it increases with increase in sintering temperature and shows highest value for the sintering temperature 800^0C.

References:

[1] M. Mozaffari, J. Amighian; Preparation of Al-substituted Ni ferrite powders via mechnochemical processing; J. Magn. Magn. Mater. 260 (2003) 244-249.

[2] N. Ponpandian, P. Balaya, A. Narayanasamy; Electrical conductivity and dielectric behaviour of nanocrystalline $NiFe_2O_4$ spinel; J. Phys: Condensed Matter 14 (2002) 3221.

[3] L. Torres, M. Zazo, A. G. Flores, V. Raposos, J. Iniguez; Study of the frequency dependence of the ferromagnetic resonance linewidths of nickel ferrites from 8-60 GHZ; J. Appl. Phys. 79 (1996) 5422.

[4] R. H. Kodama, A. E. Berkowitz, E. J. McNiff, S. Foner; Surface spin disorder in $NiFe_2O_4$ nanoparticles; Phys. Rev. Lett. 77 (1996) 394.

[5] T. M. Meaz, S. M. Attia, A. M. Abo El Ata; Effect of trivalent titanium ions substitution on the dielectric properties of Co-Zn ferrite; J. Magn. Magn. Mater. 257 (2003) 296-305.

[6] A. M. El. Sayed, Electrical conductivity of nickel – zinc and Cr substituted nickel – zinc ferrites; Mater. Chem. Phys. 82 (2003) 583-587.

[7] T. George, A. T. Sunny, T. Varghese; Magnetic properties of cobalt ferrite nanoparticles synthesized by sol-gel method; Mater. Sci. Engg. (IOP conf. series) 73 (2015) 012050.

[8] C. E. Demirci, P. K. Manna, Y. Wroczynskyj, S. Akurk, J. V. Lierop; Lanthanum ion substituted cobalt ferrite nanoparticles and their hyperthermia efficiency; J. Magn. Magn. Mater. 458 (2018) 253-260.

[9] A. G. Bhosale, B. K. Chougule; X-ray, infrared and magnetic studies of Al-substituted Ni ferrites; Mater. Chem. Phys. 97 (2006) 273-276.

[10] M. Kisielewski, A. Maziewski, M. Takielak, J. Ferre, S. Lemerle, V. Mathet, C. Chappert; Magnetic anisotropy and magnetization reversal processes in Pt/Co/Pt films; J. Magn. Magn. Mater. 260 (2003) 231-243.

[11] M. Houshiar, F. Zebhi, Z. J. Raazi, A. Alidoust, Z. Askari; Synthesis of cobalt ferrite ($CoFe_2O_4$) nanoparticles using combustion, co-precipitation and precipitation methods: A comparison study of size, structural and magnetic properties; J. Magn. Magn. Mater. 371 (2014) 43-48.

[12] G. Mustafa, M. U. Islam, W. Zhang, Y. Jamil, M. Asif Iqbal, M. Hussain, M. Ahmed; Temperature dependent structural and magnetic properties of cerium substituted Co-Cr ferrite prepared by auto combustion method.

[13] M. A. Amer, T. M. Meaz, A. G. Mostafa, H. F. El-Ghazally; Annealing effect on the structural and magnetic properties of the $CuAl_{0.6}Cr_{0.2}Fe_{1.2}O_4$ nano-ferrites; Mater. Res. Bull. 67 (2015) 207-214.

[14] A. M. Wahba, M. B. Mohamed; Structural, magnetic and dielectric properties of nanocrystalline Cr-substituted $Co_{0.8}Ni_{0.2}Fe_2O_4$ ferrite; Ceram. Inter. 40 (2014) 6127-6135.

[15] R. H. Kadam, S. T. Alone, A. S. Gaikwad, A. P. Birajdar, S. E. Shirsath; Al^{3+} ions dependent structural and magnetic properties of Co-Ni nano alloys; J. Nanosci. Nanotech. 13 (2013) 1-7.

[16] D. T. Nguyet, N. P. Duong, L. T. Hung, T. D. Hien, T. Satoh; Crystallization and magnetic behaviour of nanosized nickel ferrite prepared by citrate precursor method; J. Alloys Comp. 509 (2011) 6621-6625.

[17] Vivek Choudhari, R. H. Kadam, M. L. Mane, S. E. Shirsath, A. B. Kadam, D. R. Mane; Effect of La^{3+} impurity on magnetic and electrical properties of Co-Cu-Cr-Fe- nanoparticles; J. Nanosci. Nanotech. 14 (2014) 1-8.

[18] M. V. Choudhari, R. H. Kadam, S. B. Shelke, S. E. Shirsath, A. B. Kadam, D. R. Mane; Combustion synthesis of Co^{2+} substituted $Li_{0.5}Cr_{0.5}Fe_2O_4$ nano-powder: physical and magnetic interactions; Powder Technology 259 (2014) 14-21.

[19] G. Mustafa, M. U. Islam, W. Zhang, Y. Jamil, M. A. Iqbal, M. Hussain, M. Ahmed; Temperature dependent structural and magnetic properties of Cerium substituted Co-Cr ferrite prepared by auto-combustion method; J. Magn. Magn. Mater. 378 (2015) 409-416.

[20] H. M. I. Abdallah, T. Moyo, J. Z. Msomi; The effect of annealing temperature on the magnetic properties of $Mn_xCo_{1-x}Fe_2O_4$ ferrite nanoparticles; J. Super. Nov. Magn. DOI 10.1007/s10948-011-1231-4.

[21] M. A. Amer, T. M. Meaz, A. G. Mostafa, H. F. El-Ghazally; Annealing effect on the structural and magnetic properties of the $CuAl_{0.6}Cr_{0.2}Fe_{1.2}O_4$ nano-ferrite; Mater. Res. Bull. 67 (2015) 207-204.

[22] R. Kambale, P. Shaikh, N. Hatale, V. Bilur, Y. Korekar, C. Bhosale, K. Y. Rajpure; Structural and magnetic properties of $Co_{1-x}Mn_xFe_2O_4$ ($0<x<0.4$) spinel ferrites synthesized by combustion method; J. Alloy. Comp. 490 (2010) 568.

[23] E. Manova, B. Kunev, D. Paneva, I. Mitov, L. Petrov, C. Estournes, C. Orlean, J. Rehspringe, M. Kurmoo; Mechano-synthesis, characterization, and magnetic properties of nanoparticles of cobalt ferrite, Chem. Mater. 16 (2004) 5689-5696.